TISSUE ENGINEERING: Part A
Volume 19, Numbers 9 and 10, 2013

DOI: 10.1089/ten.tea.2012.0281

Stromal Cell Identity Influences the *In Vivo* Functionality of Engineered Capillary Networks Formed by Co-delivery of Endothelial Cells and Stromal Cells

Stephanie J. Grainger, PhD, Bita Carrion, PhD, Jacob Ceccarelli, MS, and Andrew J. Putnam, PhD

A major translational challenge in the fields of therapeutic angiogenesis and tissue engineering is the ability to form functional networks of blood vessels. Cell-based strategies to promote neovascularization have been widely explored, and have led to the consensus that co-delivery of endothelial cells (ECs) (or their progenitors) with some sort of a supporting stromal cell type is the most effective approach. However, the choice of stromal cells has varied widely across studies, and their impact on the functional qualities of the capillaries produced has not been examined. In this study, we injected human umbilical vein ECs alone or with normal human lung fibroblasts (NHLFs), human bone marrow-derived mesenchymal stem cells (BMSCs), or human adipose-derived stem cells (AdSCs) in a fibrin matrix into subcutaneous pockets in SCID mice. All conditions yielded new human-derived vessels that inosculated with mouse vasculature and perfused the implant, but there were significant functional differences in the capillary networks, depending heavily on the identity of the co-delivered stromal cells. EC-alone and EC-NHLF implants yielded immature capillary beds characterized by high levels of erythrocyte pooling in the surrounding matrix. EC-BMSC and EC-AdSC implants produced more mature capillaries characterized by less extravascular leakage and the expression of mature pericyte markers. Injection of a fluorescent tracer into the circulation also showed that EC-BMSC and EC-AdSC implants formed vasculature with more tightly regulated permeability. These results suggest that the identity of the stromal cells is key to controlling the functional properties of engineered capillary networks.

Introduction

Therapeutic angiogenesis, the process of promoting neovascularization and tissue repair via the delivery of pro-angiogenic molecules, has been explored as a possible means to treat ischemic diseases.[1] However, clinical trials relying on bolus injection of individual factors have been disappointing,[2] perhaps due to the limited half-life of most protein growth factors, the lack of temporal and spatial control over growth factor release, and the inability of single factors to properly regulate neovascularization.[3,4] Newer strategies involving sustained delivery of pro-angiogenic factors or genes from biodegradable scaffolds to overcome protein stability issues,[5–8] as well as delivery of multiple pro-angiogenic factors in a time-dependent fashion to mimic the process of natural vessel development,[4,9] have been shown to induce formation of vascular networks. However, even combinations of multiple factors may not fully recapitulate the complex milieu of pro-angiogenic signals presented to cells *in vivo*.

Cell-based therapies have also been explored to more completely mimic the cascade of signals needed to promote the formation of stable neovasculature. These approaches involve delivering appropriate cell types that can directly differentiate into capillary structures or provide a physiologic mixture of pro-angiogenic cues to accelerate the recruitment of host vessels. A variety of cell types have been shown to form new capillary networks and/or induce collateral blood vessel development after implantation *in vivo*.[10–13] In addition, cells have been implanted using a wide range of scaffold materials and extracellular matrix proteins to improve cell retention and engraftment.[14,15] However, most studies have relied on the presence of red blood cells in lumen-like structures revealed via histology as the sole metric of vessel functionality.

A particular challenge for the tissue-engineering community is to induce vascularization of ischemic tissues with blood vessels that are functionally normal. When vascularization is induced too rapidly, as in tumor angiogenesis, endothelial cells (ECs) do not properly align.[16,17] Blood vessel growth induced by tumor expansion often results in abnormal branching and growth patterns, defective endothelial wall structures, and an abnormal pericyte coat.[18] These abnormal characteristics relative to healthy vasculature can

Department of Biomedical Engineering, University of Michigan, Ann Arbor, Michigan.

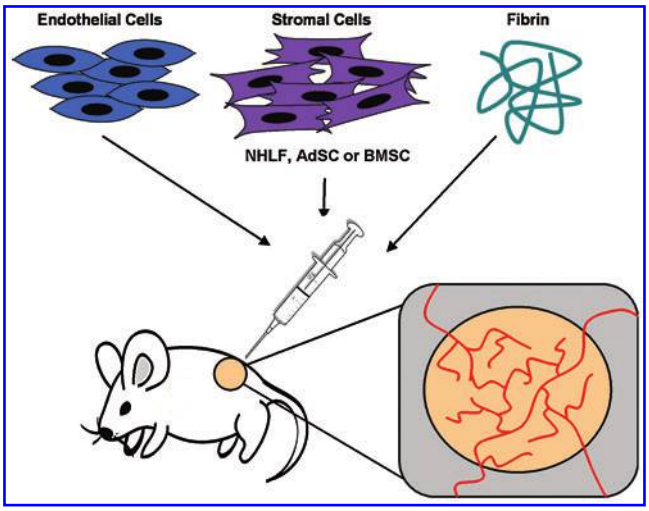

FIG. 1. Method to engineer vascular networks *in vivo*. In this study, EC alone or in combination with one of three different types of stromal cells (NHLFs, AdSCs, or BMSCs) were injected subcutaneously within a fibrin matrix on the dorsal surface of SCID mice. Injected cells form a provisional vascular network that inosculates with the systemic circulation. AdSC, adipose-derived stem cell; BMSC, bone marrow-derived mesenchymal stem cell; EC, endothelial cell; NHLF, normal human lung fibroblast. Color images available online at www.liebertpub.com/tea

lead to capillaries that are leaky and unable to properly control permeability, contributing to edema in the tissue.[19,20] In the case of engineered capillary networks, our laboratory and many others have had some previous success in inducing capillary growth in both 3D *in vitro* cultures,[21] and *in vivo* subcutaneous implants.[22] The results from such studies have led to the consensus that co-delivery of ECs and a secondary mesenchymal cell type produces the necessary cues to induce tubular sprouting of ECs, and stromal cell differentiation toward a pericytic phenotype.[23]

Despite the consensus of this paradigm, there is virtually no consensus with respect to the choice of cells to co-deliver with ECs. A variety of stromal cell types of mesenchymal origins have been explored, including mesenchymal stem cells from bone marrow[21,24,25] or adipose tissue,[26,27] fibroblasts from human lung,[28,29] and mouse embryos,[30] as well as smooth muscle cells.[31] For a subset of these cell types, our previous studies using *in vitro* models have shown that stromal cell identity underlies differences in the mechanisms by which capillaries are formed,[24,26] and in the functional properties of the resulting capillaries.[32] The goal of this study was to determine if the identity of the stromal cells co-delivered with ECs had any similar consequences on the functional properties of engineered capillary networks *in vivo* (Fig. 1). Our results suggest that the identity of the stromal cells significantly influences the *in vivo* functionality of engineered capillary networks.

Materials and Methods

Cell culture

Human umbilical vein endothelial cells (HUVECs, hereafter referred to as ECs) were harvested from fresh umbilical cords following a previously established protocol,[21] and were grown in a fully supplemented endothelial growth medium (EGM-2; Lonza) at 37°C and 5% CO_2. Normal human lung fibroblasts (NHLFs; Lonza) were cultured in Media 199 (Invitrogen) supplemented with 10% fetal bovine serum (FBS), 1% penicillin/streptomycin (Mediatech), and 0.5% gentamicin (Invitrogen). Bone marrow-derived mesenchymal stem cells (BMSCs; Lonza, passage 2) were tested by the manufacturer for purity by flow cytometry and for their ability to differentiate into osteogenic, chondrogenic, and adipogenic lineages. Cells are positive for the cell surface markers CD105, CD166, CD29 (integrin β1), and CD44, and negative for CD14, CD34, and CD45. Both BMSCs and adipose-derived stem cells (AdSCs; Invitrogen) were cultured in the Dulbecco's modified Eagle's Medium (DMEM; Sigma-Aldrich) supplemented with 10% FBS, 1% penicillin/streptomycin (Mediatech), and 0.5% gentamicin (Invitrogen). NHLFs, BMSCs, and AdSCs were all used before passage 10. ECs were used at passage 3. Cells were cultured in monolayers until reaching 80% confluency and serially passaged using 0.05% trypsin–EDTA treatment.

Tissue-construct implantation

Animal procedures were performed in accordance with the NIH guidelines for laboratory animal usage following a protocol approved by the University of Michigan's Committee on Use and Care of Animals. Male 7-week-old C.B.-17/SCID mice (Taconic Labs) were used for all experiments. An anesthetic/analgesic drug cocktail of ketamine (95 mg/kg; Fort Dodge Animal Health), xylazine (9.5 mg/kg; Lloyd Laboratories), and buprenorphine (0.059 mg/kg; Bedford Laboratories) was delivered to each mouse via intraperitoneal injection. The dorsal flank of each mouse was then shaved, sterilized with betadine (Thermo Fisher Scientific), and wiped down with an alcohol pad before implant injection.

A 2.5 mg/mL bovine fibrinogen solution (Sigma-Aldrich) was made in serum-free EGM-2 and filtered through a 0.22-μm syringe filter. Cell mixtures in a 1:1 ratio of EC:stromal cells (NHLFs, BMSCs, or AdSCs) were spun down and resuspended in the previously prepared fibrinogen solution at a final concentration of 10 million cells/mL, totaling 3 million cells per injection sample (300 μL total volume). Immediately before injection, 5% FBS and 6 μL of thrombin solution (50 U/mL; Sigma-Aldrich) were added to 300 μL of fibrinogen–cell solution. For control samples, 3 million ECs without any stromal cell type were used. Acellular controls containing fibrinogen, FBS, and thrombin were also included. Solutions were immediately injected subcutaneously on the dorsal flank of the mouse, with two implants per animal. Animals were kept stationary for 5 min to allow for implant polymerization, and were then placed in fresh cages for recovery. Five replicates of each sample type were completed (EC-NHLF, EC-BMSC, EC-AdSCs, EC only, and acellular). Surgeons were not blinded to the experimental conditions. Implants were retrieved after 7 or 14 days, consistent with the time points used in several other neovascularization studies.[9,33–36]

Noninvasive laser Doppler perfusion imaging

At days 3, 7, 10, and 14, mice were anesthetized using the cocktail described above, and then subjected to laser Doppler

perfusion imaging (LDPI; Perimed AB). Each mouse was imaged in triplicate. Results are reported as folds increased in relative perfusion units over untreated controls.

Tracer injection and implant removal

Mature capillaries function as selectively permeable membranes and are known to be impermeable to dextrans over a molecular weight of 65 kDa.[37] Therefore, a 70-kDa Texas Red-conjugated dextran ($\lambda_{ex/em}$ of 595/615 nm; Invitrogen) was chosen as a functionally defining tracer. This dextran molecule, containing free lysines, is fixable in 4% PFA. At each retrieval time point, final LDPI was completed, and each mouse was placed in a restraint device, and 200 μL of a 5% dextran solution in PBS was then injected via the tail vein. After injection, mice were placed into fresh cages, and the tracer was allowed to circulate systemically for 10 min. Animals were then euthanized, and implants, including the surrounding skin and muscle layers, were surgically excised.

Whole-mount live imaging

Explants were placed onto Petri dishes after removal and immediately imaged using an Olympus IX81 spinning-disk confocal microscope (Olympus) with both a Hamamatsu camera for visualization of the fluorescent dextran tracer (Supplementary Fig. S1; Supplementary Data are available online at www.liebertpub.com/tea), and a DP2-Twain (Olympus) camera for color bright-field images. Macroscopic images were taken using a Kodak EasyShare Z1015 IS camera (Kodak).

Histology and immunohistochemistry

For histology and immunohistochemical staining, explants were fixed in 4% PFA for 1 h, 0.4% PFA overnight, and then transferred to a PBS, pH 7.4, solution, all at 4°C. All samples were forwarded to AML Laboratories for sectioning. Samples were embedded in paraffin by AML, and then sectioned in 5-μm sections and stained with hematoxylin and eosin (H&E) according to standard protocols. All sample identities were masked to the tissue processor. hCD31, alpha-smooth muscle actin (α-SMA), and calponin were immunohistochemically stained in our laboratory on unstained serial sections provided by AML. Paraffin sections were rehydrated according to a standard protocol[22] and then steamed in a vegetable steamer for 25 min in an antigen retrieval solution (Dako). Slides were equilibrated in TBS-T, and then a DakoEnVision System-HRP (DAB) kit (Dako) was used for all subsequent staining. The primary antibody (human anti-mouse CD31; Dako, human anti-mouse α-SMA; Abcam, or human anti-mouse calponin; Abcam) was diluted 1:50 in TBS-T and incubated at 4°C overnight. Slides were then treated with an HRP-conjugated anti-mouse secondary antibody provided in the kit, followed by H&E counterstaining. Negative controls using the secondary antibody alone were generated in parallel to ensure that nonspecific staining did not occur.

Immunofluorescent staining

For fluorescent staining, explanted tissue samples were initially incubated in 30% sucrose for 48 h at 4°C. They were then transferred to a solution containing one part optimal cutting temperature (OCT) embedding compound (Andwin Scientific), and two parts 30% sucrose for another 24 h. Each sample was then finally embedded in 100% OCT within a disposable plastic mold (Fisher Scientific), and flash-frozen on the surface of liquid nitrogen. These frozen samples were then forwarded to AML Laboratories for cryosectioning in 5-μm sections. Frozen sections returned to our laboratory were prewarmed for 20 min at 25°C. Slides were submerged in PBS, pH 7.4, for three separate 5 min washes, and then blocked using 5% goat serum in PBS to eliminate nonspecific protein binding. The primary antibody (anti-rabbit human CD31; Santa Cruz Biotechnologies) was diluted 1:50 in 5% goat serum and incubated at 4°C overnight. After incubation, the unbound antibody was removed with three washes of 5 min each with PBS. The secondary antibody (Alexa Fluor-488 goat anti-rabbit; Invitrogen) at a 1:100 concentration was incubated for 30 min at room temperature. The unbound antibody was removed with three washes of 5 min each with PBS. Slides were then covered with VectaShield (Vector Labs) and a #1 glass coverslip.

Image analysis program for quantification

A customized MATLAB algorithm, described previously,[32] was modified to quantify the relative amounts of fluorescent dextran within vessel lumens and the interstitial spaces of the tissue implant. Briefly, images of the green channel (Alexa Fluor 488-hCD31) were first used to determine the location of the implanted human ECs. Using hCD31-positive staining as a guide, the capillaries within the implants in each tissue section were then identified and traced manually by the researchers; H&E-stained serial sections were used to confirm the location of the capillaries based on the presence of host erythrocytes within well-defined lumens. The red channel (Texas Red–dextran) was then overlayed, and the percentages of its localization, either within the capillaries or external to the capillaries, were determined using the following algorithm.

$$R_i = \textit{total red(inside and outside)of vessel } i$$

$$r_i = \textit{total red inside of vessel } i$$

Therefore, for a single vessel, the red outside is $r_i' = R_i - r_i$ (where r′ is the total red outside of the lumens). The total red outside of all the vessels in the image is represented as follows:

$$\sum_{i=1}^{n} R_i - r_i$$

This quantity was then normalized to the overall red (inside and out) within each image to yield a metric representing the quantity of fluorescent signal outside of the lumens.

$$\bar{r}' = \frac{\sum_{i=1}^{n} R_i - r_i}{\sum_{i=1}^{n} R_i}$$

Note that since $\sigma R \alpha n$ (the numbers of vessels), normalizing the extralumenal signal by the overall fluorescent intensity of the image accounts for variations in size, shape, and numbers of vessels.

Quantification of average number of vessels per field of view

Using hCD31-stained slides, the number of blood vessels derived from implanted cells was quantified manually. Blood vessels were identified if they exhibited a rim of positive hCD31 stain and a hollow lumen containing erythrocytes. Three sections, with five randomly taken images per section at 20×, were used to achieve statistical significance, and evaluators were masked to the experimental conditions. All values were normalized to represent a 1-mm^2 area.

Statistical analysis

All statistical analyses were performed using GraphPad Prism (GraphPad Software). Data were reported as mean ± standard deviation. Two-way analysis of variance was performed with a Newman–Keuls multiple comparison post-test. Statistical significance was assumed when $p < 0.05$.

Results

Co-injection of ECs with supporting stromal cells restored perfusion

In this study, ECs alone or in combination with one of three different types of stromal cells (NHLFs, AdSCs, or BMSCs) were injected subcutaneously within a fibrin matrix on the dorsal surface of SCID mice as depicted schematically in Figure 1. LDPI was used to noninvasively quantify blood perfusion after subcutaneous injection of one of five treatment groups. LDPI was first performed on all mice before implantation to provide a baseline control value of dorsal vascular perfusion. It was then performed again on days 3, 7, 10, and 14 post-implantation. As shown in Figure 2, relative perfusion values increased over the course of the experiment for all treatment groups; however, key differences were seen among different conditions. Co-delivery of ECs with AdSCs, BMSCs, or NHLFs within a fibrin matrix successfully restored blood flow to preinjection levels within 7 days. The restored level of perfusion was maintained at 14 days for these multicellular implants. By comparison, delivery of ECs alone partially restored blood flow by 7 days, but perfusion dropped off in the subsequent 7 days. Acellular fibrin gels failed to restore perfusion to preinjection levels within 14 days.

Live implant imaging qualitatively confirmed perfusion of the neovasculature

Immediately after implant removal, whole-mount live imaging was performed, revealing some qualitative, yet striking, differences in the appearance of the explanted tissues (Fig. 3). At day 7, all of the retrieved implants were red, perhaps indicative of connecting to the host vasculature, although the implant from the EC-NHLF condition was notably the most red (Fig. 3A). The visible redness suggests erythrocyte leakage into the implant. After 14 days (Fig. 3B), the bright red color remained present in the EC-alone and EC-NHLF conditions; by contrast, the red color diminished in the EC-AdSC and EC-BMSC implants. Implants for these latter two conditions were pale pink/yellow color in macroscopic appearance by day 14, yet retained easily identifiable blood vessels that were bright red in color. At this later time point, the fibrin also appeared somewhat more compacted and perhaps more degraded in the EC-alone and EC-NHLF conditions.

Stromal cells of different origins produced vessels with distinct morphologies

Images of the H&E-stained day-7 and day-14 explants revealed additional qualitative differences in the morphologies of the vessels formed in the various experimental groups (Fig. 4). Stained sections from the day-7 EC-only implants contained many large vessel-like structures, but these structures lacked consistent, circumscribed geometry, and the implants contained obvious extravascular erythrocytes (Fig. 4A). Significant vessel regression and matrix degradation were apparent by day 14 (Fig. 4B). The cells that remained in the fibrin by day 14 were mainly spindle-shaped free ECs, and there was little evidence of organization into capillary structures. EC-NHLF implants also

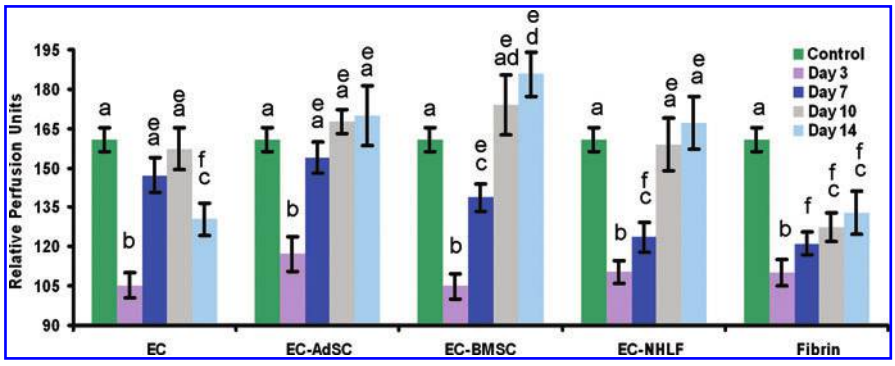

FIG. 2. Subcutaneous co-injection of EC and supporting stromal cells within fibrin matrices restore perfusion better than delivery of EC alone. Laser Doppler perfusion imaging was used to noninvasively quantify blood perfusion after subcutaneous injection of one of five treatment groups (all within fibrin gels): ECs, EC-AdSCs, EC-BMSCs, EC-NHLFs, or fibrin alone. a, b, c, and d denote statistically significant differences ($p < 0.05$) within each experimental group (i.e., a is different than b, etc.). e and f indicate statistically significant differences ($p < 0.05$) across the different experimental groups (i.e., e is different than f across groups, but all the e's are statistically the same). Color images available online at www.liebertpub.com/tea

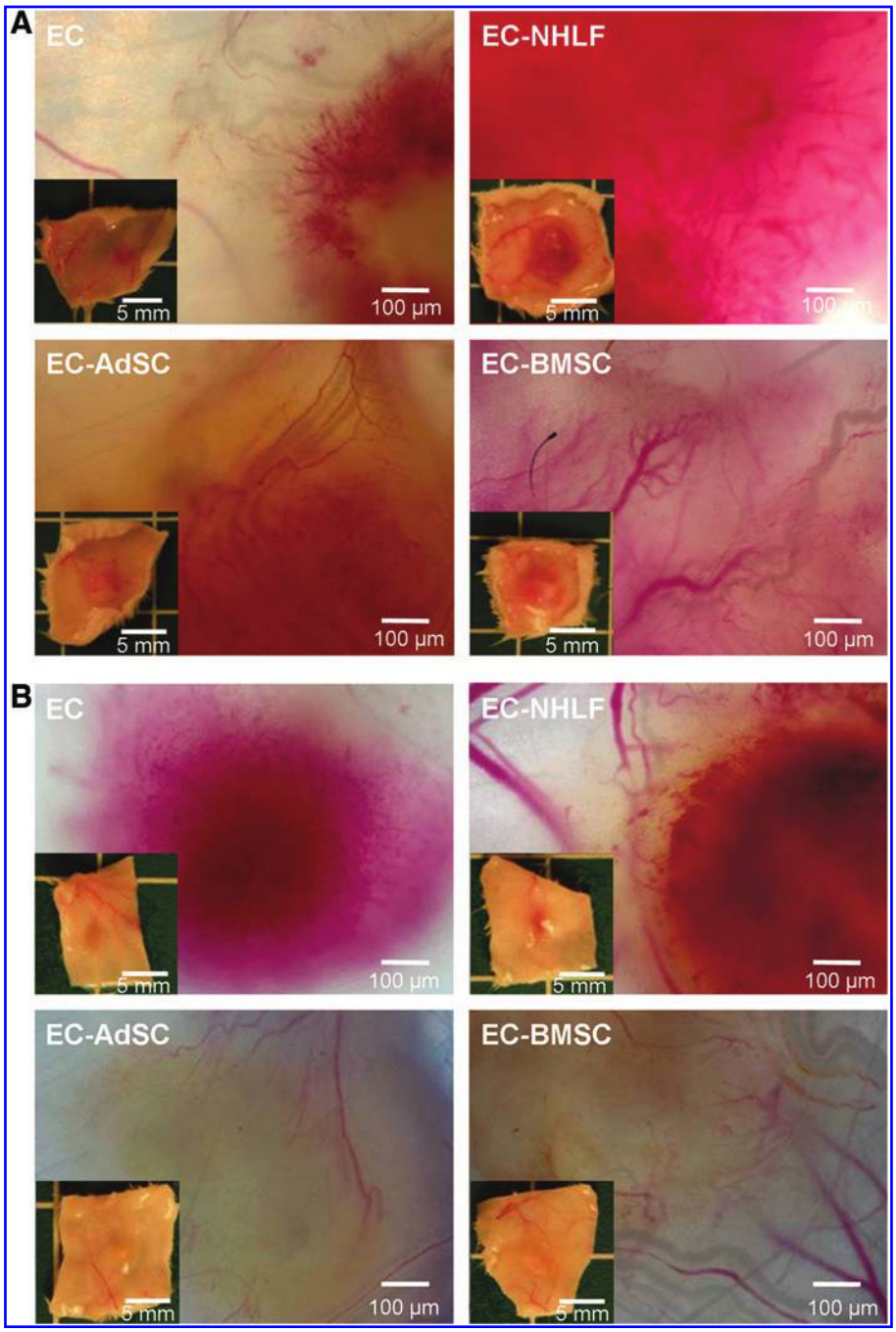

FIG. 3. Whole-mount live imaging shows perfusion of implant neovessels. Explants of each treatment group imaged as live whole-mounts at **(A)** day 7 and **(B)** day 14. Insets are macroscopic photographs. Color images available online at www.liebertpub.com/tea

contained many immature, interconnected blood vessels at day 7 (Fig. 4A), but it was difficult to discern clear vessel boundaries due to the somewhat chaotic and irregular shapes of the vessel-like structures and large amounts of matrix reorganization. After 14 days, there appeared to be a qualitative decrease in the amount of free erythrocytes in the explanted EC-NHLF tissues, but some still remained. By contrast, implants containing the multipotent stromal cells (AdSCs or BMSCs) yielded starkly different results. These samples contained many small capillaries with very well-defined lumens, circumscribed borders, and very few free erythrocytes. These capillaries were distributed throughout the entire implant to produce a vascularized, homogeneous implant containing both large and small blood vessels throughout to effectively supply the tissue with oxygenated blood.

Immunohistochemical staining for human CD31 validated the observations from the H&E-stained sections, and confirmed the human origins of the neovasculature (Fig. 5). In the implants containing ECs only, there was a diffuse brown stain indicating an abundance of human ECs and some lumen-like structures, especially at day 7 (Fig. 5A). The EC-NHLF implants showed many elongated vessel-like structures. By contrast, the EC-BMSC and EC-AdSC implants contained many smaller, tightly sealed capillaries, consistent with the observations from H&E staining. Quantification of

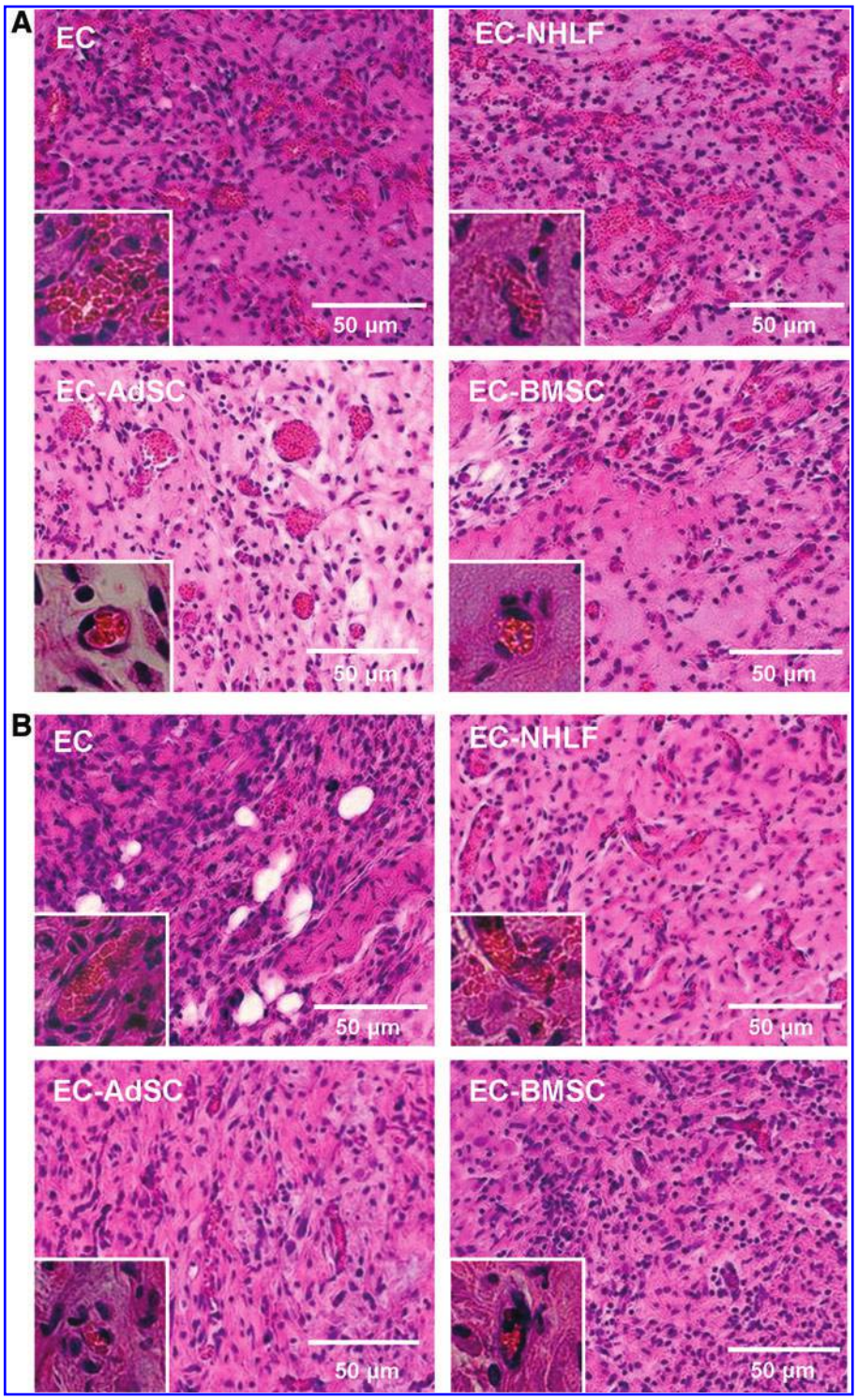

FIG. 4. Histological staining illustrates varying blood vessel morphologies in implants across treatment groups. Histologically stained sections of implants retrieved at **(A)** day 7 or **(B)** day 14 post-injection. Insets are higher-magnification (60×) micrographs to more clearly show vessel morphologies. Color images available online at www.liebertpub.com/tea

vascular density from these types of images supported these qualitative observations. Specifically, EC-only implants contained 46±3 vessels per mm^2 at 7 days, but this value dropped to 9±2 vessels per mm^2 by day 14. EC-NHLF implants contained 47±6 vessels per mm^2 at day 7, which was reduced to 31±2 vessels per mm^2 by day 14. Relative to these two conditions, the EC-AdSC and EC-BMSC implants produced fewer numbers of blood vessels. EC-AdSC implants contained 29±7 and 19±4 vessels per mm^2 at days 7 and 14, respectively. EC-BMSC implants formed 20±4 and 13±3 vessels per mm^2 at days 7 and 14, respectively. Acellular fibrin implants showed little evidence of vascularization or host network invasion (see Supplementary Fig. S1). By 14 days post-implantation, the fibrin implants had been resorbed by the host, and normal host dorsal vasculature was observed at the implantation site.

Stromal cells with multilineage potential express markers of mature smooth muscle

One possible explanation for the observed differences in vessel morphology is that the multipotent stromal cells may possess the ability to differentiate into pericytes, or even mature smooth muscle cells, while the fibroblasts cannot. To assess this possibility in our experimental system, we stained histological sections for two different markers—α-SMA and calponin (Fig. 6). α-SMA has been widely used as a pericyte marker,[18] whereas calponin is a marker of mature smooth muscle.[38] IHC staining of human α-SMA revealed a broadly positive result for all of the implants containing a co-delivered stromal cell type, particularly at day 7 (Fig. 6A). By day 14, this positive staining had somewhat decreased across all multicellular implants. In the EC-BMSC and EC-AdSC implants, positive α-SMA staining was circumferentially localized around the newly developed blood vessels, while the

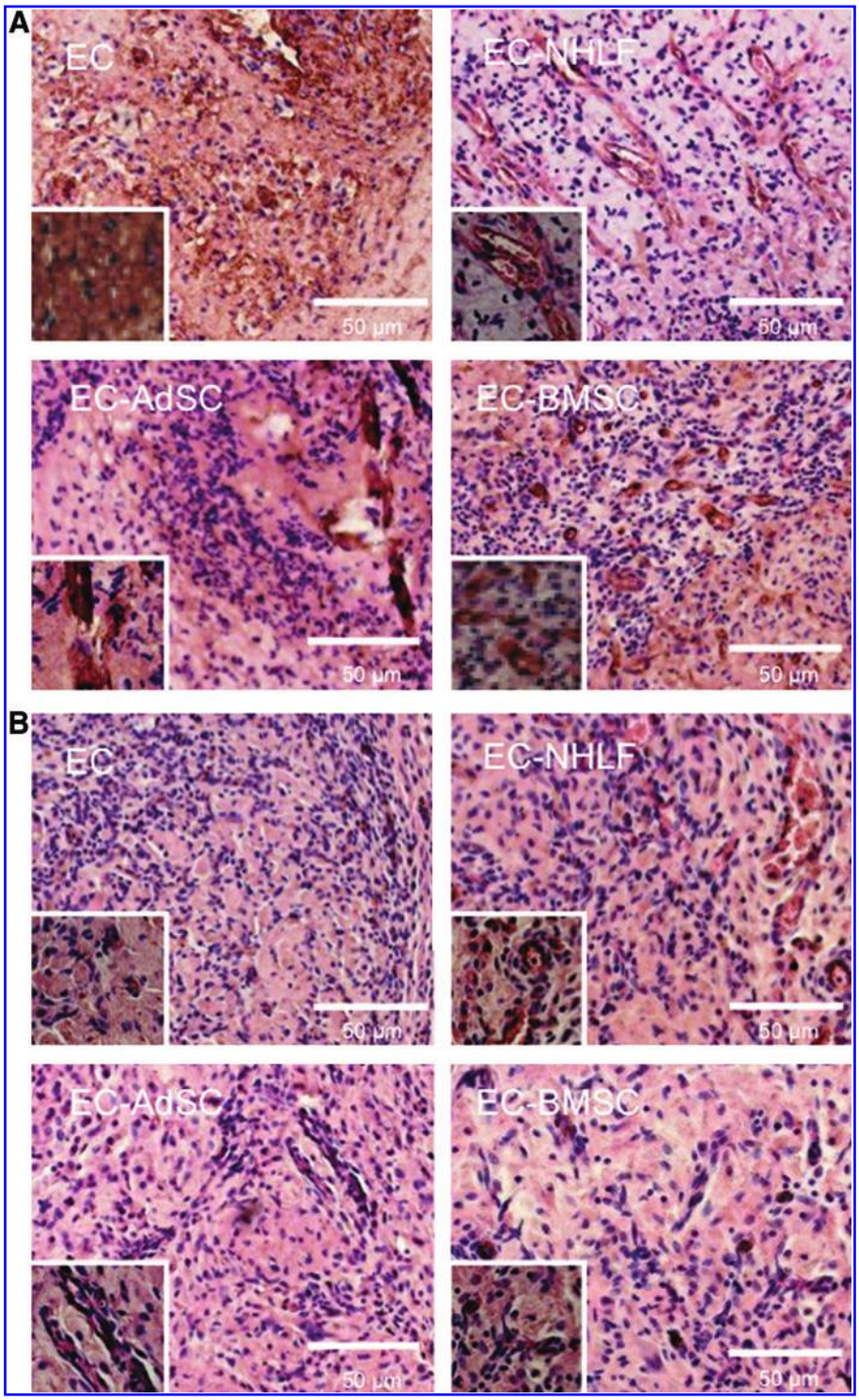

FIG. 5. Human CD31 staining confirms blood vessel origin. hCD31 staining of implants at either **(A)** day 7 or **(B)** day 14 post-implantation. All samples have been counterstained with H&E. Insets are higher-magnification (60×) micrographs to more clearly show vessel morphologies. **(C)** Quantification of images from **(A)** and **(B)**. In the graph, "a" denotes statistical significance ($p < 0.05$) between time points within an experimental group. Across experimental groups, data marked with different letters are statistically different ($p < 0.05$) (i.e., "b" is different than "c"), while those marked with the same letters are not (i.e., differences across all of the "b's" are insignificant). H&E, hematoxylin and eosin. Color images available online at www.liebertpub.com/tea

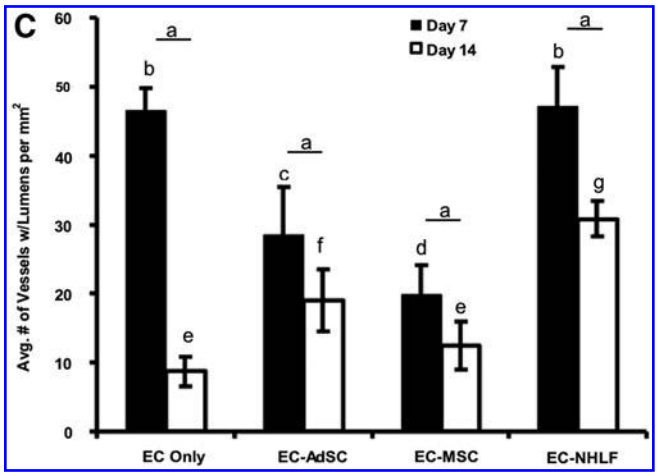

FIG. 5. (Continued).

EC-NHLF implants contained a more diffuse positive staining of cells throughout the matrix. By contrast, calponin staining was only positive at day 14 in the implants containing AdSCs or BMSCs (Fig. 7, particularly panel B). These results suggest that while NHLFs, AdSCs, and BMSCs are all capable of promoting the formation of vasculature and expressing α-SMA, only the multipotent AdSCs and BMSCs are capable of differentiating into a mature smooth muscle phenotype that is the hallmark of a larger and more mature vasculature.

Stromal cell presence and identity alter the functional permeability of the neovessels

The data presented thus far suggest that all 3 stromal cell types—NHLFs, AdSCs, and BMSCs—are capable of promoting the formation of vasculature in subcutaneous pockets when co-delivered with ECs. The histological findings hint at possible functional differences in the neovessels that form, but nearly all of the observed differences have been qualitative, subjective, and frankly unsatisfying. Therefore, in the final part of this study, we sought to determine how the inclusion of the stromal cells and their various identities quantitatively affects the functional properties of engineered capillary networks.

Based on some recent *in vitro* findings, we hypothesized that the resistance to permeability of the nascent vessels would strongly depend on stromal cell identity.[32] To quantify the relative permeabilities of the vasculature formed *in vivo*, a 70-kDa fluorescent dextran molecule was injected via tail vein in the various experimental animals (systemic injection of the functionally defining tracer can be seen at the host–implant interface in Supplementary Fig. S2). Inclusion of either AdSCs or BMSCs in the implants resulted in much tighter control of permeability relative to the other conditions (Fig. 8). In the EC-only and EC-NHLF groups, a significant fraction of the fluorescent dextran was observed outside of the vessel borders (defined by the green CD31 staining), and freely diffused throughout the implant tissue (Fig. 8A). By comparison, the EC-AdSC and EC-BMSC groups contained very well-defined vessels in which the Texas Red–dextran was circumscribed by human-CD31+ cells, with significantly less red signal in the surroundings. Importantly, we had also previously developed and validated an automated MATLAB-based image-processing algorithm to quantify vessel permeability.[32] When we applied this algorithm to quantify the relative fluorescence contained with lumens as described in the Materials and Methods section, the resulting data confirmed that co-delivery of ECs with AdSCs or BMSCs yields vessels whose control of permeability is superior (Fig. 8B).

Discussion

This study examined the quantity and functional quality of engineered capillary networks formed via co-delivery of ECs with one of three types of supporting stromal cells (NHLFs, BMSCs, or AdSCs) in a fibrin-based subcutaneous implant. Fibrin is a naturally occurring biopolymer that acts as the provisional matrix during wound healing in the human body, and has been widely shown in the literature to support neovascularization.[22,33,35,39,40] The animal model used here has also been widely exploited in the literature to approximate wound healing and test the ability of transplanted human cells to form vasculature,[19,22,29,33–35] in part because the human cells injected into SCID mice are not rejected.

We focused our efforts on NHLFs, BMSCs, and AdSCs as the stromal cell types in large part because of our own prior *in vitro* work,[24,26,32] which has suggested some differences in the mechanisms by which these cells promote vascularization. However, the use of these three types of stromal cells has been gaining traction in the tissue-engineering literature in recent years. In the case of fibroblasts, their co-delivery with stem cell-derived cardiomyocytes and ECs has been explored in the context of vascularized cardiac patches.[41] A high density of cotransplanted NHLFs, in particular, in a prevascularized tissue construct has been shown to accelerate the rate of inosculation between host vessels and the implanted vessels.[29] Likewise, AdSCs co-delivered with ECs in collagen-based implants have been shown to enhance vascularization, and to help sustain pancreatic islets or adipocytes.[34] There are also a number of studies that have explored the utility of BMSCs co-delivered with ECs to build functional vasculature.[22,25]

The results presented here show that all four of the experimental groups (EC-alone, EC-NHLFs, EC-AdSCs, and EC-BMSCs) yielded new human-derived vessels that inosculated with mouse vasculature and perfused the implant with blood. However, functional differences in the capillary networks were also revealed, depending on the identity of the co-delivered stromal cells. Importantly, the observed differences in vessel function were not apparent in data generated by manually counting numbers of vessels in H&E- or hCD31-stained histological sections, the most common endpoint utilized to assess functional connections between implanted capillary beds and the host vasculature.

LDPI was also used to assess blood flow, and provided an indirect indication of inosculation between the host vessels and the newly developed vasculature within the implant. This method has been widely employed in the tissue-engineering literature to assess the success of revascularization therapies.[42,43] The main advantages of this technology are its noninvasive and real-time measuring capabilities. In our study, mice were anesthetized for a short period and

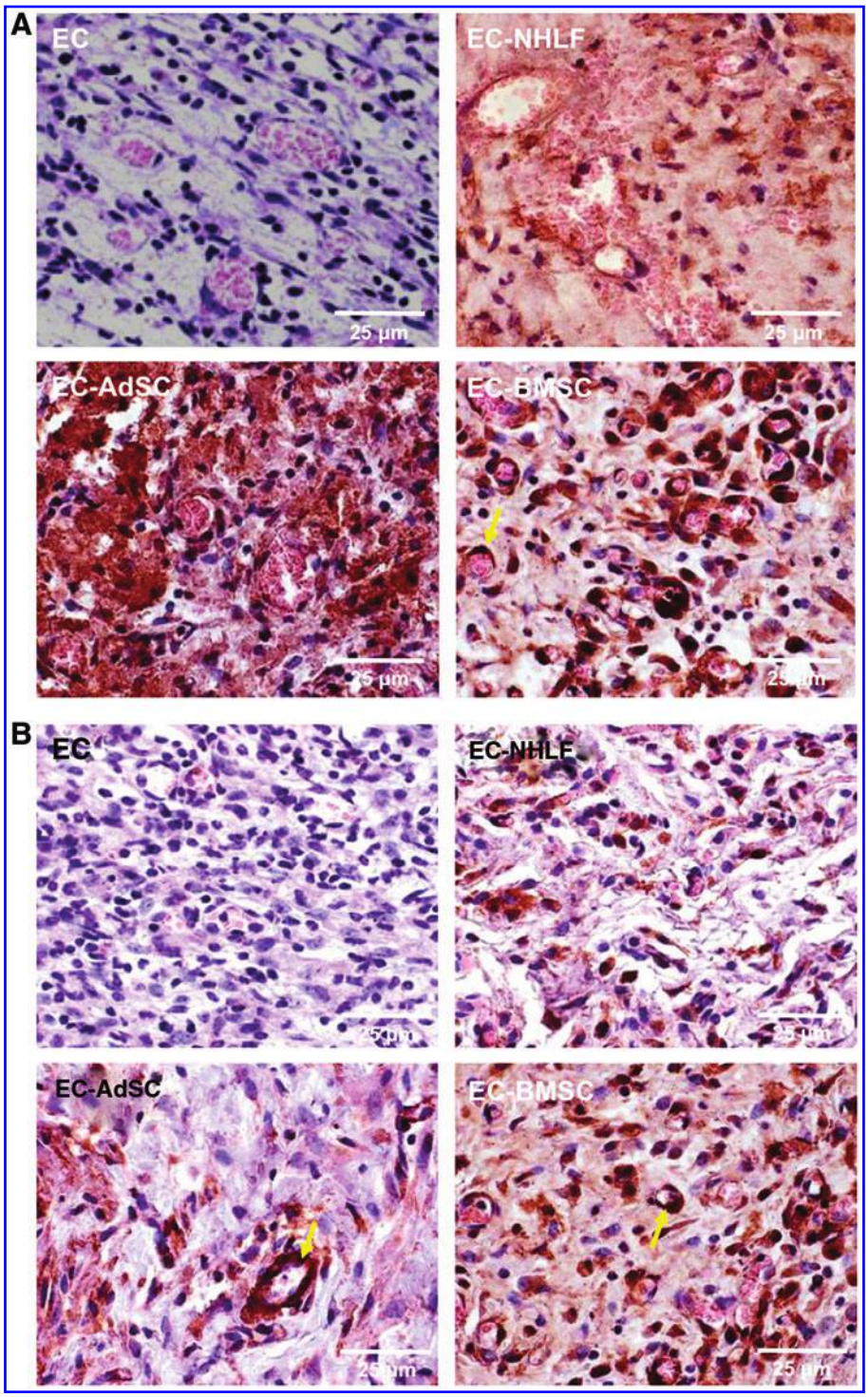

FIG. 6. α-SMA staining identifies stromal cells within the implant. Human α-SMA staining (brown) and counterstaining with H&E at **(A)** 7 days and **(B)** 14 days post-implantation. Arrows point to representative positive α-SMA around vessels, but prevalent positive staining is present in all implants that contain stromal cells at both time points. α-SMA, alpha-smooth muscle actin. Color images available online at www.liebertpub.com/tea

experiments performed longitudinally across multiple time points with the same mouse. However, LDPI results may be somewhat misleading, as the data in Figure 2 suggest. Specifically, we found that co-delivery of ECs with AdSCs, BMSCs, or NHLFs within a fibrin matrix successfully restored blood flow to preinjection levels, with no significant differences between them. Delivery of ECs alone partially restored blood flow by 7 days, but perfusion dropped off in the ensuing 7-day period. From these data alone, one might conclude that AdSCs, BMSCs, and NHLFs are all equal with respect to their ability to promote functional vessels that can perfuse an implant. However, erythrocyte pooling and edema into the implants could not be quantified via LDPI.

Macroscopic images (Fig. 3) suggested some differences across the different experimental groups. EC-NHLF implants were visibly red to the naked eye, especially at the day-7 timepoint. EC-BMSC and EC-AdSC implants were significantly lighter in color by comparison. Implants containing only ECs were somewhere in between in gross appearance. H&E staining of the retrieved implants (Fig. 4) revealed

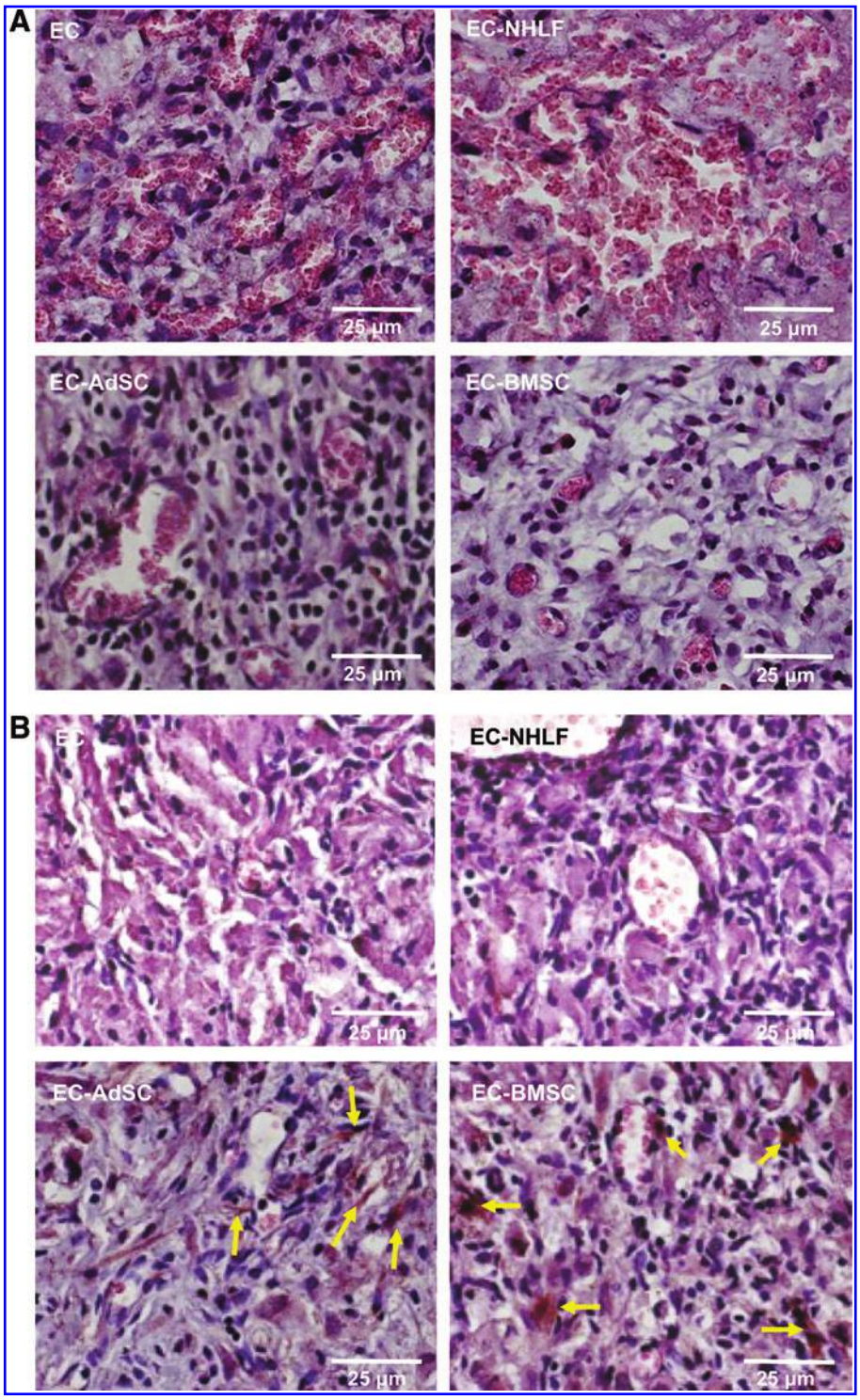

FIG. 7. Calponin staining identifies mature smooth muscle cells within the implant. Calponin staining (brown) and counterstaining with H&E at **(A)** 7 days and **(B)** 14 days post-implantation. Arrows point to representative positive calponin around vessels, which is only observed in EC-BMSC and EC-AdSC conditions at day 14. Color images available online at www.liebertpub.com/tea

many free erythrocytes within the EC-only and EC-NHLF implants. The presence of multipotent stromal cells, from either bone marrow or adipose, yielded smaller, more well-defined blood vessels throughout the implants. These vessels appeared to be tightly lined with ECs, as identified by the hCD31 staining (Fig. 5A, B). However, manual quantification of perfused lumen-containing structures on these hCD31-stained sections (Fig. 5C) seemed to suggest that EC-NHLF co-delivery was superior to EC-BMSC or EC-AdSC co-delivery in terms of numbers of vessels. Implants containing ECs alone also appeared to yield greater numbers of vessels initially, but these vessels were unstable in the absence of a co-delivered stromal cell. In fact, it was only when we assessed the permeability of the engineered vessel networks by systemically injecting a fluorescent tracer into the host circulation that the functional superiority of co-delivering ECs with the multipotent stromal cells emerged. As shown in Figure 8, a significant fraction of the Texas Red–dextran

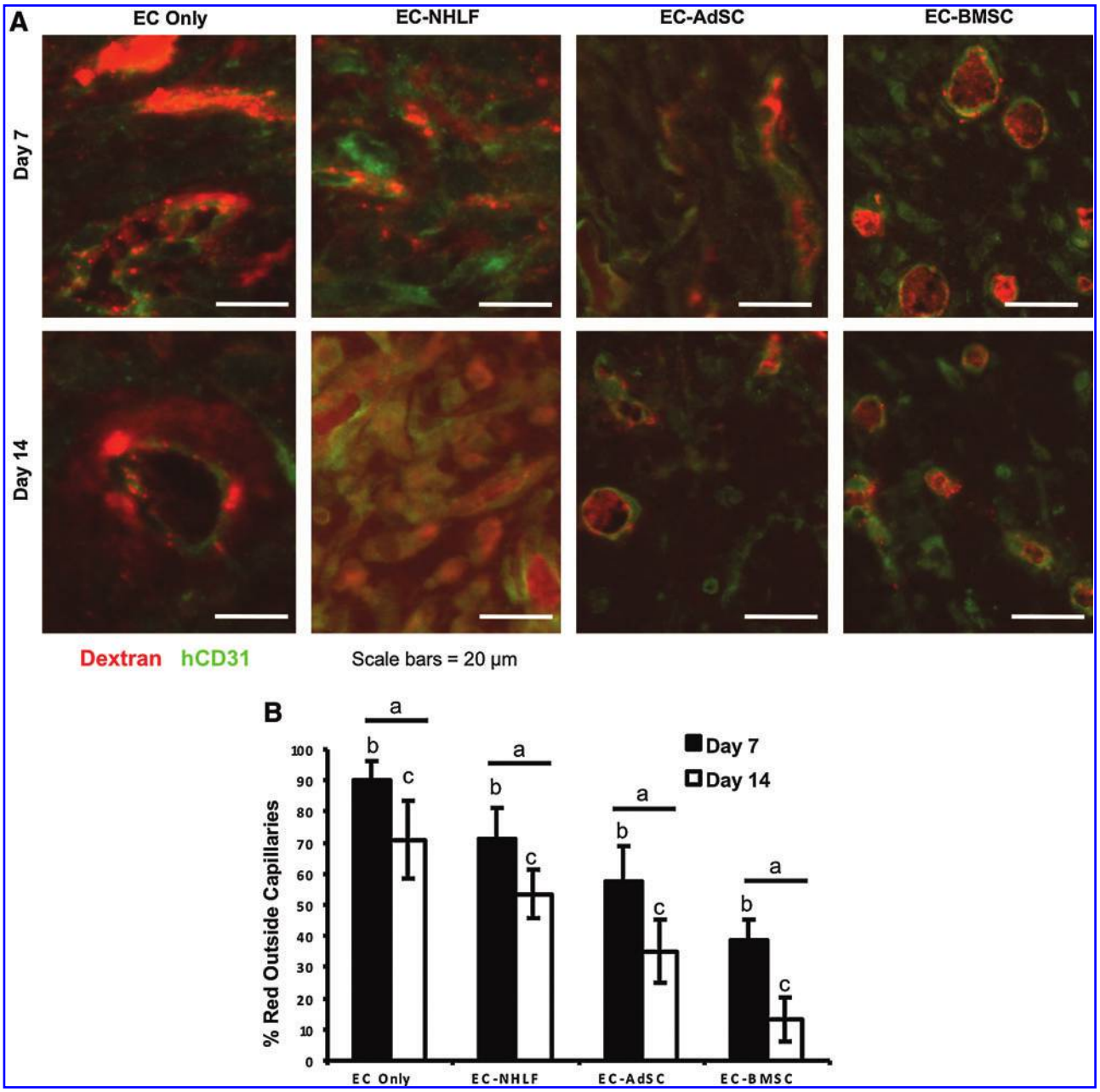

FIG. 8. Co-injection of ECs with AdSCs or BMSCs yields neovasculature with superior functional properties. **(A)** SCID mice were subjected to tail vein injections of 70-kDa Texas Red–dextran (red) tracer to visualize inosculation and characterize vessel leakiness. Tissues were counterstained with anti-human CD31 antibodies (green) to verify the human origins of the vessels. **(B)** Quantitative results of the relative amounts of red tracer both inside and outside of capillary vessels achieved using a custom MATLAB image-processing algorithm. In the graph, "a" denotes statistical significance ($p < 0.05$) between time points within an experimental group. Across experimental groups, data marked with either "b" or "c" are statistically different ($p < 0.05$) from other data marked with the same letter (i.e., all of the "b's" are different from each other). Color images available online at www.liebertpub.com/tea

leaked outside of the vessel borders in the EC-only and EC-NHLF groups, especially at the day-7 timepoint. By comparison, the fluorescent dextran was better retained with the vessels in the EC-AdSC and EC-BMSC groups.

There are numerous possible explanations for the superior functional properties of the vessels created in the EC-AdSC and EC-BMSC groups. One possibility is that the multipotent AdSCs and BMSCs are capable of differentiating into pericytes, and perhaps even functional smooth muscle, while the NHLFs are not. However, assessing this possibility is difficult due to the limited availability of *bona fide* pericyte markers. Smooth muscle α-actin is commonly used as a pericyte marker,[44,45] but it is also a marker of myofibroblasts.[46] In our results, the EC-only condition is negative for α-SMA, but all of the other conditions show some degree of positive staining (Fig. 6). The EC-NHLF implants show several small, stippled areas of positive staining. By contrast, only the EC-AdSC and EC-BMSC implants show positive

calponin staining, an indication of possible smooth muscle differentiation, and only after 14 days (Fig. 7), implying evolvement of a smooth muscle-like phenotype of implanted stromal cells. Together, these two pieces of data suggest that the AdSCs and BMSCs may be able to differentiate into functional pericytes, and eventually smooth muscle cells, and thus are better able to stabilize the new vessel networks and modulate their permeability. By contrast, the terminally differentiated NHLFs (and perhaps fibroblasts, more generally) act more as myofibroblasts in a wound-healing environment, rapidly promoting vessel formation to heal the wound. Prior results from an *in vitro* comparison of these different stromal cell types show that NHLFs promote capillary morphogenesis at a faster rate,[32] consistent with this possible explanation.

A second possibility is that the various stromal cell types survive to differing degrees after implantation. This could lead to different numbers of stromal cells, which may in turn affect the number and quality of the resulting vessels that form. A third possibility is that the various stromal cell types secrete distinct pro- and antiangiogenic cytokines that regulate vessel maturation, and/or differentially contribute to the production of new ECM proteins required for vessel formation and stability.[47] A final possibility relates to the influence of stromal cell identity on the proteolytic remodeling of the ECM during the neovascularization process.[24,48] Our published data suggest that capillary formation induced by fibroblasts is very fast (perhaps tumor-like), resulting from a plasmin-mediated proteolysis that rapidly degrades the matrix and disrupts its mechanical properties in a global fashion. By contrast, BMSCs and AdSCs induce a much more focal, strategic matrix remodeling that is MT1-MMP dependent and results in capillaries that form more slowly, but also in a more stable manner. These kinetic differences in capillary morphogenesis controlled by matrix breakdown ultimately determine the functional permeability and stability of the resulting vasculature. An essential step in our ongoing efforts to evaluate this hypothesis was to show that stromal cell identity does indeed regulate vessel quality *in vivo*, as we have done here. However, we do not yet have any definitive experimental data that allow us to dismiss any of these or other potential mechanisms.

In conclusion, the results of this study suggest that the identity of the stromal cells co-delivered with ECs is key to controlling the functional properties of vasculature engineered via cell delivery, and argue that multipotent stromal cells with the ability to differentiate *in situ* are superior to terminally differentiated fibroblasts. Importantly, this study also underscores the need for more quantifiable metrics of functionality, rather than relying solely on the manual counting of the numbers of vessels in histological sections.

Acknowledgments

The authors would like to thank Dr. Troy Lau for assistance in writing the customized MATLAB algorithm, and Dr. J. Erby Wilkinson of the University of Michigan Unit for Laboratory Animal Medicine, for assistance in interpreting the histology slides. This work was partially supported by the National Institutes of Health (Grant Nos. R01-HL085339 and R01-HL085339-03S1). S.J.G. was supported by a predoctoral fellowship from the NIH Cellular Biotechnology Training Grant (T32-GM-008353).

Disclosure Statement

No competing financial interests exist.

References

1. Ferrara, N., and Alitalo, K. Clinical applications of angiogenic growth factors and their inhibitors. Nat Med **5,** 1359, 1999.
2. Davis, B.H., Schroeder, T., Yarmolenko, P.S., Guilak, F., Dewhirst, M.W., and Taylor, D.A. An *in vitro* system to evaluate the effects of ischemia on survival of cells used for cell therapy. Ann Biomed Eng **35,** 1414, 2007.
3. Chen, R.R., Silva, E.A., Yuen, W.W., Brock, A.A., Fischbach, C., Lin, A.S., Guldberg, R.E., and Mooney, D.J. Integrated approach to designing growth factor delivery systems. FASEB J **21,** 3896, 2007.
4. Sun, Q., Silva, E.A., Wang, A., Fritton, J.C., Mooney, D.J., Schaffler, M.B., Grossman, P.M., and Rajagopalan, S. Sustained release of multiple growth factors from injectable polymeric system as a novel therapeutic approach towards angiogenesis. Pharm Res **27,** 264, 2010.
5. Lee, K.Y., Peters, M.C., Anderson, K.W., and Mooney, D.J. Controlled growth factor release from synthetic extracellular matrices. Nature **408,** 998, 2000.
6. Murphy, W.L., and Mooney, D.J. Controlled delivery of inductive proteins, plasmid DNA and cells from tissue engineering matrices. J Periodontal Res **34,** 413, 1999.
7. Sun, Q., Chen, R.R., Shen, Y., Mooney, D.J., Rajagopalan, S., and Grossman, P.M. Sustained vascular endothelial growth factor delivery enhances angiogenesis and perfusion in ischemic hind limb. Pharm Res **22,** 1110, 2005.
8. Zisch, A.H., Lutolf, M.P., Ehrbar, M., Raeber, G.P., Rizzi, S.C., Davies, N., Schmokel, H., Bezuidenhout, D., Djonov, V., Zilla, P., and Hubbell, J.A. Cell-demanded release of VEGF from synthetic, biointeractive cell ingrowth matrices for vascularized tissue growth. FASEB J **17,** 2260, 2003.
9. Richardson, T.P., Peters, M.C., Ennett, A.B., and Mooney, D.J. Polymeric system for dual growth factor delivery. Nat Biotechnol **19,** 1029, 2001.
10. Iba, O., Matsubara, H., Nozawa, Y., Fujiyama, S., Amano, K., Mori, Y., Kojima, H., and Iwasaka, T. Angiogenesis by implantation of peripheral blood mononuclear cells and platelets into ischemic limbs. Circulation **106,** 2019, 2002.
11. Kinnaird, T., Stabile, E., Burnett, M.S., Shou, M., Lee, C.W., Barr, S., Fuchs, S., and Epstein, S.E. Local delivery of marrow-derived stromal cells augments collateral perfusion through paracrine mechanisms. Circulation **109,** 1543, 2004.
12. Pesce, M., Orlandi, A., Iachininoto, M.G., Straino, S., Torella, A.R., Rizzuti, V., Pompilio, G., Bonanno, G., Scambia, G., and Capogrossi, M.C. Myoendothelial differentiation of human umbilical cord blood-derived stem cells in ischemic limb tissues. Circ Res **93,** e51, 2003.
13. Rehman, J., Traktuev, D., Li, J., Merfeld-Clauss, S., Temm-Grove, C.J., Bovenkerk, J.E., Pell, C.L., Johnstone, B.H., Considine, R.V., and March, K.L. Secretion of angiogenic and antiapoptotic factors by human adipose stromal cells. Circulation **109,** 1292, 2004.
14. Nor, J.E., Christensen, J., Mooney, D.J., and Polverini, P.J. Vascular endothelial growth factor (VEGF)-mediated angiogenesis is associated with enhanced endothelial cell sur-

vival and induction of Bcl-2 expression. Am J Pathol **154,** 375, 1999.
15. Nor, J.E., Peters, M.C., Christensen, J.B., Sutorik, M.M., Linn, S., Khan, M.K., Addison, C.L., Mooney, D.J., and Polverini, P.J. Engineering and characterization of functional human microvessels in immunodeficient mice. Lab Invest **81,** 453, 2001.
16. Baluk, P., Hashizume, H., and McDonald, D.M. Cellular abnormalities of blood vessels as targets in cancer. Curr Opin Genet Dev **15,** 102, 2005.
17. Carmeliet, P., and Jain, R.K. Angiogenesis in cancer and other diseases. Nature **407,** 249, 2000.
18. Jain, R.K. Normalization of tumor vasculature: an emerging concept in antiangiogenic therapy. Science **307,** 58, 2005.
19. Melero-Martin, J.M., De Obaldia, M.E., Kang, S.Y., Khan, Z.A., Yuan, L., Oettgen, P., and Bischoff, J. Engineering robust and functional vascular networks in vivo with human adult and cord blood–derived progenitor cells. Circ Res **103,** 128, 2008.
20. Hashizume, H., Baluk, P., Morikawa, S., McLean, J.W., Thurston, G., Roberge, S., Jain, R.K., and McDonald, D.M. Openings between defective endothelial cells explain tumor vessel leakiness. Am J Pathol **156,** 1363, 2000.
21. Ghajar, C.M., Blevins, K.S., Hughes, C.C., George, S.C., and Putnam, A.J. Mesenchymal stem cells enhance angiogenesis in mechanically viable prevascularized tissues via early matrix metalloproteinase upregulation. Tissue Eng **12,** 2875, 2006.
22. Kniazeva, E., Kachgal, S., and Putnam, A.J. Effects of extracellular matrix density and mesenchymal stem cells on neovascularization *in vivo*. Tissue Eng Part A **17,** 905, 2011.
23. Bergers, G., and Song, S. The role of pericytes in blood-vessel formation and maintenance. Neuro-Oncol **7,** 452, 2005.
24. Ghajar, C.M., Kachgal, S., Kniazeva, E., Mori, H., Costes, S.V., George, S.C., and Putnam, A.J. Mesenchymal cells stimulate capillary morphogenesis via distinct proteolytic mechanisms. Exp Cell Res **316,** 813, 2010.
25. Au, P., Tam, J., Fukumura, D., and Jain, R.K. Bone marrow-derived mesenchymal stem cells facilitate engineering of long-lasting functional vasculature. Blood **111,** 4551, 2008.
26. Kachgal, S., and Putnam, A.J. Mesenchymal stem cells from adipose and bone marrow promote angiogenesis via distinct cytokine and protease expression mechanisms. Angiogenesis **14,** 47, 2011.
27. Merfeld-Clauss, S., Gollahalli, N., March, K.L., and Traktuev, D.O. Adipose tissue progenitor cells directly interact with endothelial cells to induce vascular network formation. Tissue Eng Part A **16,** 2953, 2010.
28. Ghajar, C.M., Chen, X., Harris, J.W., Suresh, V., Hughes, C.C., Jeon, N.L., Putnam, A.J., and George, S.C. The effect of matrix density on the regulation of 3-D capillary morphogenesis. Biophys J **94,** 1930, 2008.
29. Chen, X., Aledia, A.S., Popson, S.A., Him, L., Hughes, C.C., and George, S.C. Rapid anastomosis of endothelial progenitor cell-derived vessels with host vasculature is promoted by a high density of cotransplanted fibroblasts. Tissue Eng Part A **16,** 585, 2010.
30. Motegi, S., Leitner, W.W., Lu, M., Tada, Y., Sardy, M., Wu, C., Chavakis, T., and Udey, M.C. Pericyte-derived MFG-E8 regulates pathologic angiogenesis. Arterioscler Thromb Vasc Biol **31,** 2024, 2011.
31. Shepherd, B.R., Jay, S.M., Saltzman, W.M., Tellides, G., and Pober, J.S. Human aortic smooth muscle cells promote arteriole formation by coengrafted endothelial cells. Tissue Eng Part A **15,** 165, 2009.
32. Grainger, S.J., and Putnam, A.J. Assessing the permeability of engineered capillary networks in a 3D culture. PLoS One **6,** e22086, 2011.
33. Chen, X., Aledia, A.S., Ghajar, C.M., Griffith, C.K., Putnam, A.J., Hughes, C.C., and George, S.C. Prevascularization of a fibrin-based tissue construct accelerates the formation of functional anastomosis with host vasculature. Tissue Eng Part A **15,** 1363, 2009.
34. Traktuev, D.O., Prater, D.N., Merfeld-Clauss, S., Sanjeevaiah, A.R., Saadatzadeh, M.R., Murphy, M., Johnstone, B.H., Ingram, D.A., and March, K.L. Robust functional vascular network formation *in vivo* by cooperation of adipose progenitor and endothelial cells. Circ Res **104,** 1410, 2009.
35. Allen, P., Melero-Martin, J., and Bischoff, J. Type I collagen, fibrin and PuraMatrix matrices provide permissive environments for human endothelial and mesenchymal progenitor cells to form neovascular networks. J Tissue Eng Regen Med **5,** e74, 2011.
36. Melero-Martin, J.M., Khan, Z.A., Picard, A., Wu, X., Paruchuri, S., and Bischoff, J. *In vivo* vasculogenic potential of human blood-derived endothelial progenitor cells. Blood **109,** 4761, 2007.
37. Curry, F.E., Huxley, V.H., and Adamson, R.H. Permeability of single capillaries to intermediate-sized colored solutes. Am J Physiol **245,** H495, 1983.
38. Hughes, S., and Chan-Ling, T. Characterization of smooth muscle cell and pericyte differentiation in the rat retina *in vivo*. Invest Ophthalmol Vis Sci **45,** 2795, 2004.
39. Ehrbar, M., Djonov, V.G., Schnell, C., Tschanz, S.A., Martiny-Baron, G., Schenk, U., Wood, J., Burri, P.H., Hubbell, J.A., and Zisch, A.H. Cell-demanded liberation of VEGF121 from fibrin implants induces local and controlled blood vessel growth. Circ Res **94,** 1124, 2004.
40. Hiraoka, N., Allen, E., Apel, I.J., Gyetko, M.R., and Weiss, S.J. Matrix metalloproteinases regulate neovascularization by acting as pericellular fibrinolysins. Cell **95,** 365, 1998.
41. Stevens, K.R., Kreutziger, K.L., Dupras, S.K., Korte, F.S., Regnier, M., Muskheli, V., Nourse, M.B., Bendixen, K., Reinecke, H., and Murry, C.E. Physiological function and transplantation of scaffold-free and vascularized human cardiac muscle tissue. Proc Natl Acad Sci U S A **106,** 16568, 2009.
42. Phelps, E.A., Landazuri, N., Thule, P.M., Taylor, W.R., and Garcia, A.J. Bioartificial matrices for therapeutic vascularization. Proc Natl Acad Sci U S A **107,** 3323, 2010.
43. Silva, E.A., Kim, E.S., Kong, H.J., and Mooney, D.J. Material-based deployment enhances efficacy of endothelial progenitor cells. Proc Natl Acad Sci U S A **105,** 14347, 2008.
44. Bexell, D., Gunnarsson, S., Tormin, A., Darabi, A., Gisselsson, D., Roybon, L., Scheding, S., and Bengzon, J. Bone marrow multipotent mesenchymal stroma cells act as pericyte-like migratory vehicles in experimental gliomas. Mol Ther **17,** 183, 2009.
45. Shi, S., and Gronthos, S. Perivascular niche of postnatal mesenchymal stem cells in human bone marrow and dental pulp. J Bone Miner Res **18,** 696, 2003.
46. Hinz, B. Formation and function of the myofibroblast during tissue repair. J Invest Dermatol **127,** 526, 2007.
47. Newman, A.C., Nakatsu, M.N., Chou, W., Gershon, P.D., and Hughes, C.C. The requirement for fibroblasts in angiogenesis: fibroblast-derived matrix proteins are essential for endothelial cell lumen formation. Mol Biol Cell **22,** 3791, 2011.

48. Kachgal, S., Carrion, B., Janson, I.A., and Putnam, A.J. Bone marrow stromal cells stimulate an angiogenic program that requires endothelial MT1-MMP. J Cell Physiol **227,** 3546, 2012.
49. Schechner, J.S., Nath, A.K., Zheng, L., Kluger, M.S., Hughes, C.C., Sierra-Honigmann, M.R., Lorber, M.I., Tellides, G., Kashgarian, M., Bothwell, A.L., and Pober, J.S. *In vivo* formation of complex microvessels lined by human endothelial cells in an immunodeficient mouse. Proc Natl Acad Sci U S A **97,** 9191, 2000.

Address correspondence to:
Andrew J. Putnam, PhD
Department of Biomedical Engineering
University of Michigan
2154 Lurie Biomedical Engineering
1101 Beal Ave.
Ann Arbor, MI 48109-2110

E-mail: putnam@umich.edu

Received: May 7, 2012
Accepted: December 7, 2012
Online Publication Date: February 1, 2013

This article has been cited by:

1. Dan Zhao, Changyue Xue, Shiyu Lin, Sirong Shi, Qianshun Li, Mengting Liu, Xiaoxiao Cai, Yunfeng Lin. 2017. Notch Signaling Pathway Regulates Angiogenesis via Endothelial Cell in 3D Co-Culture Model. *Journal of Cellular Physiology* **232**:6, 1548-1558. [Crossref]
2. Sonja B. Riemenschneider, Donald J. Mattia, Jacqueline S. Wendel, Jeremy A. Schaefer, Lei Ye, Pilar A. Guzman, Robert T. Tranquillo. 2016. Inosculation and perfusion of pre-vascularized tissue patches containing aligned human microvessels after myocardial infarction. *Biomaterials* **97**, 51-61. [Crossref]
3. Yifei Du, Fei Jiang, Yi Liang, Yuli Wang, Weina Zhou, Yongchu Pan, Mingfei Xue, Yan Peng, Huan Yuan, Ning Chen, Hongbing Jiang. 2016. The angiogenic variation of skeletal site-specific human BMSCs from same alveolar cleft patients: a comparative study. *Journal of Molecular Histology* **47**:2, 153-168. [Crossref]
4. Buitinga Mijke, Janeczek Portalska Karolina, Cornelissen Dirk-Jan, Plass Jacqueline, Hanegraaf Maaike, Carlotti Françoise, de Koning Eelco, Engelse Marten, van Blitterswijk Clemens, Karperien Marcel, van Apeldoorn Aart, de Boer Jan. 2016. Coculturing Human Islets with Proangiogenic Support Cells to Improve Islet Revascularization at the Subcutaneous Transplantation Site. *Tissue Engineering Part A* **22**:3-4, 375-385. [Abstract] [Full Text HTML] [Full Text PDF] [Full Text PDF with Links]
5. Dario F. Riascos-Bernal, Prameladevi Chinnasamy, Longyue (Lily) Cao, Charlene M. Dunaway, Tomas Valenta, Konrad Basler, Nicholas E. S. Sibinga. 2016. β-Catenin C-terminal signals suppress p53 and are essential for artery formation. *Nature Communications* **7**, 12389. [Crossref]
6. Ana Y. Rioja, Ramkumar Tiruvannamalai Annamalai, Spencer Paris, Andrew J. Putnam, Jan P. Stegemann. 2016. Endothelial sprouting and network formation in collagen- and fibrin-based modular microbeads. *Acta Biomaterialia* **29**, 33-41. [Crossref]
7. Young Hye Song, Seung Hee Shon, Mengrou Shan, Abraham D Stroock, Claudia Fischbach. 2016. Adipose-derived stem cells increase angiogenesis through matrix metalloproteinase-dependent collagen remodeling. *Integrative Biology* **8**:2, 205-215. [Crossref]
8. Tobias Hasenberg, Severin Mühleder, Andrea Dotzler, Sophie Bauer, Krystyna Labuda, Wolfgang Holnthoner, Heinz Redl, Roland Lauster, Uwe Marx. 2015. Emulating human microcapillaries in a multi-organ-chip platform. *Journal of Biotechnology* **216**, 1-10. [Crossref]
9. R. Samuel, D. G. Duda, D. Fukumura, R. K. Jain. 2015. Vascular diseases await translation of blood vessels engineered from stem cells. *Science Translational Medicine* **7**:309, 309rv6-309rv6. [Crossref]
10. Christoph Patsch, Ludivine Challet-Meylan, Eva C. Thoma, Eduard Urich, Tobias Heckel, John F. O'Sullivan, Stephanie J. Grainger, Friedrich G. Kapp, Lin Sun, Klaus Christensen, Yulei Xia, Mary H. C. Florido, Wei He, Wei Pan, Michael Prummer, Curtis R. Warren, Roland Jakob-Roetne, Ulrich Certa, Ravi Jagasia, Per-Ola Freskgård, Isaac Adatto, Dorothee Kling, Paul Huang, Leonard I. Zon, Elliot L. Chaikof, Robert E. Gerszten, Martin Graf, Roberto Iacone, Chad A. Cowan. 2015. Generation of vascular endothelial and smooth muscle cells from human pluripotent stem cells. *Nature Cell Biology* **17**:8, 994-1003. [Crossref]
11. Rao Rameshwar R., Vigen Marina L., Peterson Alexis W., Caldwell David J., Putnam Andrew J., Stegemann Jan P.. 2015. Dual-Phase Osteogenic and Vasculogenic Engineered Tissue for Bone Formation. *Tissue Engineering Part A* **21**:3-4, 530-540. [Abstract] [Full Text HTML] [Full Text PDF] [Full Text PDF with Links]
12. König Julia, Weiss Gregor, Rossi Daniele, Wankhammer Karin, Reinisch Andreas, Kinzer Manuela, Huppertz Berthold, Pfeiffer Dagmar, Parolini Ornella, Lang Ingrid. 2015. Placental Mesenchymal Stromal Cells Derived from Blood Vessels or Avascular Tissues: What Is the Better Choice to Support Endothelial Cell Function?. *Stem Cells and Development* **24**:1, 115-131. [Abstract] [Full Text HTML] [Full Text PDF] [Full Text PDF with Links] [Supplemental Material]
13. Fei Jiang, Jie Ma, Yi Liang, Yuming Niu, Ning Chen, Ming Shen. 2015. Amniotic Mesenchymal Stem Cells Can Enhance Angiogenic Capacity via MMPs In Vitro and In Vivo. *BioMed Research International* **2015**, 1-15. [Crossref]
14. Marina Vigen, Jacob Ceccarelli, Andrew J. Putnam. 2014. Protease-Sensitive PEG Hydrogels Regulate Vascularization In Vitro and In Vivo. *Macromolecular Bioscience* **14**:10, 1368-1379. [Crossref]
15. Rahul Singh, Marina Vigen, Andrew Putnam. Mesenchymal Support Cells in the Assembly of Functional Vessel Networks 37-58. [Crossref]
16. Rameshwar R. Rao, Jacob Ceccarelli, Marina L. Vigen, Madhu Gudur, Rahul Singh, Cheri X. Deng, Andrew J. Putnam, Jan P. Stegemann. 2014. Effects of hydroxyapatite on endothelial network formation in collagen/fibrin composite hydrogels in vitro and in vivo. *Acta Biomaterialia* **10**:7, 3091-3097. [Crossref]
17. Thai-Yen Ling, Yen-Liang Liu, Yung-Kang Huang, Sing-Yi Gu, Hung-Kuan Chen, Choa-Chi Ho, Po-Nien Tsao, Yi-Chung Tung, Huei-Wen Chen, Chiung-Hsiang Cheng, Keng-Hui Lin, Feng-Huei Lin. 2014. Differentiation of lung stem/progenitor

cells into alveolar pneumocytes and induction of angiogenesis within a 3D gelatin – Microbubble scaffold. *Biomaterials* **35**:22, 5660-5669. [Crossref]

18. Yeasmin Shamima, Ceccarelli Jacob, Vigen Marina, Carrion Bita, Putnam Andrew J., Tarle Susan A., Kaigler Darnell. 2014. Stem Cells Derived from Tooth Periodontal Ligament Enhance Functional Angiogenesis by Endothelial Cells. *Tissue Engineering Part A* **20**:7-8, 1188-1196. [Abstract] [Full Text HTML] [Full Text PDF] [Full Text PDF with Links]
19. Jacob Ceccarelli, Andrew J. Putnam. 2014. Sculpting the blank slate: How fibrin's support of vascularization can inspire biomaterial design. *Acta Biomaterialia* **10**:4, 1515-1523. [Crossref]
20. Jinling Ma, Fang Yang, Sanne K Both, Henk-Jan Prins, Marco N Helder, Juli Pan, Fu-Zhai Cui, John A Jansen, Jeroen JJP van den Beucken. 2014. In vitro and in vivo angiogenic capacity of BM-MSCs/HUVECs and AT-MSCs/HUVECs cocultures. *Biofabrication* **6**:1, 015005. [Crossref]
21. Morin Kristen T., Dries-Devlin Jessica L., Tranquillo Robert T.. 2014. Engineered Microvessels with Strong Alignment and High Lumen Density Via Cell-Induced Fibrin Gel Compaction and Interstitial Flow. *Tissue Engineering Part A* **20**:3-4, 553-565. [Abstract] [Full Text HTML] [Full Text PDF] [Full Text PDF with Links] [Supplemental Material]
22. YJ Blinder, DJ Mooney, S Levenberg. 2014. Engineering approaches for inducing blood vessel formation. *Current Opinion in Chemical Engineering* **3**, 56-61. [Crossref]
23. Andrew J. Putnam. 2014. The instructive role of the vasculature in stem cell niches. *Biomater. Sci.* **2**:11, 1562-1573. [Crossref]
24. Yulia Shamis, Eduardo A. Silva, Kyle J. Hewitt, Yevgeny Brudno, Shulamit Levenberg, David J. Mooney, Jonathan A. Garlick. 2013. Fibroblasts Derived from Human Pluripotent Stem Cells Activate Angiogenic Responses In Vitro and In Vivo. *PLoS ONE* **8**:12, e83755. [Crossref]
25. Bita Carrion, Yen P. Kong, Darnell Kaigler, Andrew J. Putnam. 2013. Bone marrow-derived mesenchymal stem cells enhance angiogenesis via their $\alpha 6\beta 1$ integrin receptor. *Experimental Cell Research* **319**:19, 2964-2976. [Crossref]
26. Kristen T. Morin, Robert T. Tranquillo. 2013. In vitro models of angiogenesis and vasculogenesis in fibrin gel. *Experimental Cell Research* **319**:16, 2409-2417. [Crossref]